Meteoritics & Planetary Science 39, Nr 12, 1967–1981 (2004)
Abstract available online at http://meteoritics.org

Martian xenon components in Shergotty mineral separates: Locations, sources, and trapping mechanisms

K. D. OCKER* and J. D. GILMOUR[2]

[1]Institute for Rare Isotope Measurements, University of Tennessee, 10521 Research Drive, Suite 300, Knoxville, Tennessee 37932, USA
[2]Department of Earth Sciences, The University of Manchester, Manchester M13 9PL, UK
*Corresponding author's e-mail address: kdostone@utk.edu

Received 8 September 2004; revision accepted 26 September 2004

Abstract–Isotopic signatures and concentrations of xenon have been measured in Shergotty mineral separates by laser step heating. Martian atmosphere and 'martian interior' xenon are present, as is a spallation component. Martian atmospheric xenon is 5–10 times more concentrated in opaque minerals (magnetite, ilmenite, and pyrrhotite) and maskelynite than in pyroxenes, perhaps reflecting grain size variation. This is shown to be consistent with shock incorporation. A component consisting of solar xenon with a fission contribution, similar to components previously identified in martian meteorites and associated with the martian interior, is best defined in the pyroxene-dominated separates. This component exhibits a consistent ^{129}Xe (^{129}Xe/^{132}Xe ~1.2) excess over solar/planetary (^{129}Xe/^{132}Xe ~1.04). We suggest that gas present in the melt, perhaps a mixture of interior xenon and martian atmosphere, was incorporated into the pyroxenes in Shergotty as the minerals crystallized.

INTRODUCTION

It is now widely accepted that the group of meteorites historically known as the SNC (shergottites, nakhlites, and Chassigny) meteorites are martian in origin, allowing us to obtain geologic information about Earth's neighboring planet in the laboratory. The shergottites fall into two sub-groups: basalts and lherzolites. In our work, of which this paper forms part, we focus on the basaltic shergottites. These are relatively fine-grained and consist predominantly of the clinopyroxenes pigeonite and augite, with lesser amounts of maskelynite (diaplectic glass produced from plagioclase during shock), titanomagnetite, ilmenite, whitlockite, and other accessory phases and mesostasis (Smith and Hervig 1979; Stolper and McSween 1979; Stöffler et al. 1986). Their petrogenesis began with the crystallization of homogeneous, Mg-rich pigeonite and augite grains followed by the alignment of the pyroxene grains and the crystallization of Fe-rich pyroxene rims onto the magnesian pigeonite and augite cores. Crystallization of the interstitial, zoned plagioclase is also thought to have occurred at this time. The remaining trapped melt continued to crystallize, forming whitlockite, magnetite, ilmenite, and other accessory phases and mesostasis (McSween 1994).

Studies of trace elements and radiogenic isotopes in the basaltic shergottites' parent magmas have given a chronological sketch of the source regions of the shergottites. Model ages suggest that martian global differentiation, including core formation, occurred near 4.5 Ga, and was for the most part concurrent with the completion of accretion (Shih et al. 1982; Chen and Wasserburg 1986; Jagoutz 1991). This resulted in a depleted mantle and an enriched crust. Time-integrated light rare earth elements (LREE) depletions observed in the martian meteorites imply that the martian interior preserved ancient heterogeneities; this is in contrast to the earth, where convective mixing has homogenized the mantle (Jagoutz et al. 1994). The shergottites crystallized about 180 Ma ago by melting a source with Rb/Sr and U/Pb similar to the nakhlite source and with related patterns of incompatible element abundances, suggesting that basaltic shergottites sampled the same source region as the nakhlites, but at different times (Jones 1989; Longhi 1991; Jagoutz et al. 1994).

The basaltic shergottites exhibit correlated variations in rare earth element fractionation and isotopic systematics of neodymium and strontium. This suggests a mixture of two sources: one component which is identified with the depleted martian mantle, and another component which is tentatively associated with the martian crust, being relatively enriched in large ion lithophile elements (Jones 1986; Borg et al. 1997). The redox state of the meteorites also suggests a two-source mixture. In each case, Shergotty is representative of the highest contribution from the 'crustal' component. Shergotty has the highest oxygen fugacity (close to the quartz-fayalite-

magnetite oxygen buffer curve, reflecting an evolved component) and the lowest epsilon neodymium (Jones 1986). This is in contrast to Queen Alexandra Range (QUE) 94201, the meteorite with the lowest crustal component, which has oxygen fugacity close to the iron-wüstite buffer (Herd and Papike 2000) and higher ε_{Nd} (Borg et al. 1997).

Figure 1 uses literature data to illustrate the variations in the bulk xenon isotope signatures of the basaltic shergottites (Swindle et al. 1986; Ott 1988; Terribilini 2000; Mathew and Marti 2001, 2002; Mathew et al. 2003). Xenon isotope systematics of martian meteorites typically reveal a mixing between a martian atmospheric signature (Shergottite Parent Body; Swindle et al. 1986) and one or more interior components. The xenon isotopic signature of the martian atmosphere, identified in shergottite melt glass and in Nakhla, is distinguished by an elevated $^{129}Xe/^{132}Xe$ ratio of 2.40 ± 0.02 (Swindle et al. 1986). A pure solar xenon ($^{129}Xe/^{132}Xe \cong 1$) has been observed in the dunite Chassigny and is denoted here by Chass-S (Ott 1988). Its presence in a dunite led to its association with the martian interior. Further components, dominated by solar xenon but with varying proportions of fission xenon, are also identified with the martian interior. The fission source has been identified as ^{244}Pu (Mathew and Marti 2001). There is some variation in the relative proportions of fission xenon and solar xenon in these components. One such component, also detected in Chassigny (Mathew and Marti 2001) and denoted as Chass-E (Fig. 1), has a similar $^{129}Xe/^{132}Xe$ ratio to Chass-S, the pure solar interior component. Chass-E is a well-defined component, implying that fission and solar xenon were well mixed before incorporation into the meteorite, ruling out in situ decay (Mathew and Marti 2001). The estimated interior component of Allan Hills (ALH) 84001 as well as Nakhla analysis also indicate mixtures of fission and solar xenon (Mathew personal communication), albeit in distinctly different proportions from each other and from Chass-E. In these cases, the components are constrained to lie on mixing lines between solar and ^{244}Pu source, and the $^{129}Xe/^{132}Xe$ ratio in the interior component is not accurately known. In Fig. 1, literature data from bulk analyses of shergottites suggest the presence of an interior component containing some fission xenon as well as modern martian atmosphere. However, the proportions of fission and solar xenon in the interior component of the individual basaltic shergottites are not well constrained.

Xenon isotopic analyses of mineral separates from ALH 84001 and Nakhla have been reported (Gilmour et al. 2001 and references therein). In these meteorites, the atmosphere-derived xenon component is associated with a lower Kr/Xe ratio than that of the martian atmosphere (as determined in the shergottite melt glass), an elemental fractionation most readily associated with the trapping mechanism. It was determined that the majority of trapped martian atmosphere xenon measured in ALH 84001 was located in the orthopyroxenes and is believed to have been incorporated into the surface of the grains by shock (Gilmour et al. 1998). This component is isotopically distinct from the modern martian atmosphere, leading to its identification with an ancient atmosphere trapped 4 Ga ago. In Nakhla, the highest concentration of martian atmospheric xenon is associated with the feldspathic mesostasis, though mass balance suggests pyroxene is an equally significant host in the bulk meteorite (Gilmour et al. 1999). Alteration products have also been shown to host martian atmospheric xenon in the nakhlite Lafayette, though they do not contribute significantly to the overall budget (Swindle et al. 2000). This distribution has been interpreted as a grain size effect consistent with shock incorporation of martian atmospheric noble gases adsorbed onto mineral surfaces, a process that seems capable of accounting for both the observed elemental fractionation and the distribution among host phases.

Studies on the basaltic shergottites to date have been limited to bulk analysis (Fig. 1). The data are consistent with a mixture of modern martian atmospheric xenon with a martian interior component consisting of fission xenon intimately mixed with solar xenon. Here we present a xenon isotopic study of mineral separates from Shergotty to complement these bulk analyses. Our aim was to determine the location of the martian xenon components derived from the atmosphere and interior as well as to characterize the proportions of fission and solar xenon present in the interior component. In light of our results, we discuss how these components came to be incorporated into Shergotty in the context of accepted models of its crystallization and subsequent history. We also discuss wider implications for the noble gas geochemistry of Mars.

EXPERIMENTAL PROCEDURE

A 50 mg sample of Shergotty (sample number: #1985, MFH) was crushed and physically separated by hand-picking the grains that were identified by eye as dominantly consisting of pyroxene (yellow to light brown), maskelynite (clear glass), and opaques (black and with magnetite responding to a weak magnet). Based on published mineral modes (Stolper and McSween 1979), the resulting groups of pyroxene-dominated separates (Pyx-1: 7.84 mg, Pyx-2: 6.25 mg) are composed of augite and pigeonite in equal proportions and may contain trace amounts of fayalite; maskelynite-dominated separates (Msk-1: 7.28 mg) consist of the diaplectic glass and may contain trace amounts of whitlockite; and the opaque-dominated separates (Opq-1: 1.06 mg) are composed of titanomagnetite, ilmenite, and pyrrhotite. A bulk sample (WR-1: 4.19 mg) was also retained for xenon isotopic analysis.

Major element compositions (Ca, Al, Mg, and Fe) were obtained from two thick sections of Shergotty using the fully automated CAMECA SX-50 electron microscope at the

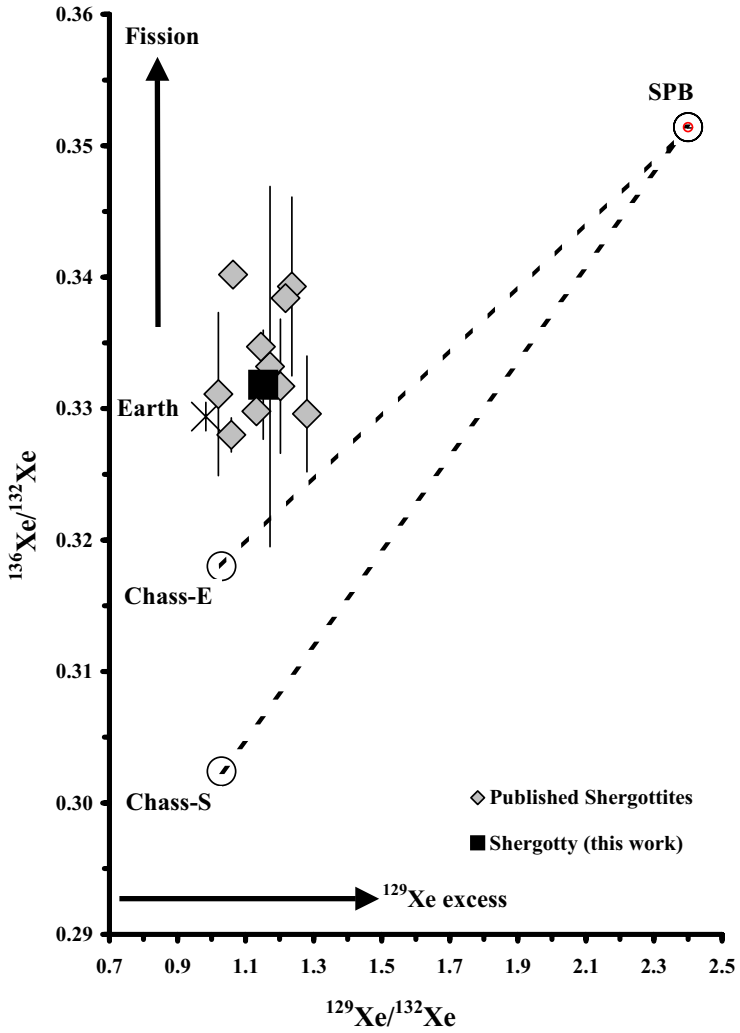

Fig. 1. The $^{136}Xe/^{132}Xe$ ratio versus $^{129}Xe/^{132}Xe$ ratio for some basaltic shergottites. The xenon composition of the basaltic shergottites has been described as a mixture of a martian atmosphere component noted as SPB for Shergottite parent body (Swindle et al. 1986) and a martian mantle-like solar component found in Chassigny (Chass-S) (Ott 1988). However, all the presented data lie above this simple two-component mixing line, suggesting three-component mixing or modification of the mantle-like component (see text). Published values of Shergotty are represented to show the agreement with our whole rock data (Swindle et al. 1986; Ott 1988; Terribilini 2000; Mathew et al. 2001; Mathew et al. 2003).

University of Tennessee, which employs an accelerating voltage of 15 kV, a beam current of 20–30 nA, and full ZAF (PAP) correction. Backscatter images (Fig. 2) and EDS analysis were used for confirmation of the different minerals present in the thick sections, which were then used to create a second series of separates: "bulk" pyroxene (Pyx-3: 2.45 mg), augite (Aug-1: 1.55 mg), pigeonite (Pig-1: 1.51 mg), and maskelynite. The maskelynite sample was further divided into two subsamples: unwashed Msk-2 (1.59 mg) and Msk-HCl (1.33 mg) that had been washed with 1% HCl (19.5 hours) to remove phosphates. Analyzing the acid solution removed from washing the maskelynite grains by ion chromatography revealed phosphate at 1.7 wt.% of the separate.

Samples were loaded into the laser port of the Refrigerator Enhanced Laser Analyzer for Xenon (RELAX) mass spectrometer (Gilmour et al. 1994) for laser step-heating. Step-heating experiments were performed using a defocused (minimum spot diameter ~200 μm) continuous wave Nd:YAG laser (1064 nm) heating for 2 min and gettering for 1 min. The sample gas was then allowed into the mass spectrometer and 5 min of xenon data acquisition was immediately performed. RELAX is a time-of-flight instrument and complete spectra are produced by summing together data acquired over 10 sec. Thus, a five minute analysis consisted of 30 consecutive spectra, each made by summing 100 individual spectra at 10 Hz. The blank level was around 1×10^{-16} ccSTP ^{132}Xe, while build-up was close to 8×10^{-16} ccSTP ^{132}Xe over the five minute data acquisition period. The data reduction proceeded as previously described (Gilmour et al. 1998).

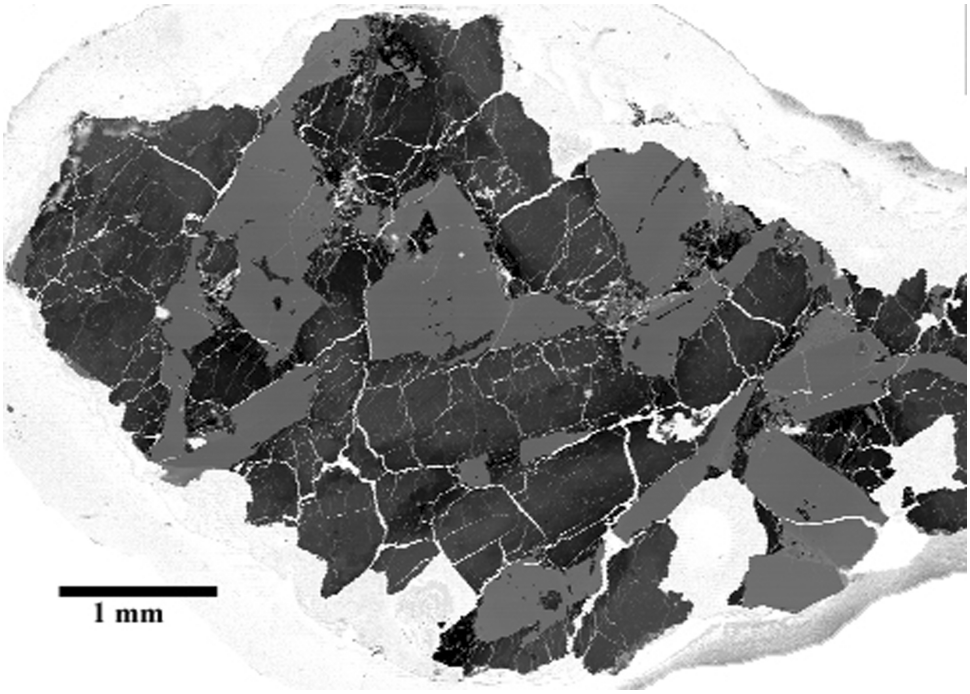

Fig. 2. Inverted backscatter image of a thick section of the Shergotty meteorite showing large pyroxene crystals separated by gray lathes of maskelynite.

RESULTS

All xenon data acquired from the analyses are presented in Table 1 and summarized in Table 2. The whole rock concentration is dominated by contributions from pyroxene and maskelynite, but even though the minor opaque phase is significantly more gas-rich, it is not present in sufficient amounts to affect the mass balance. Fig. 3a shows the laser step-heating data from the whole rock plotted with ^{129}Xe and ^{124}Xe normalized to ^{132}Xe. Elevated ^{129}Xe ratios are diagnostic of the martian atmosphere, while increased $^{124}Xe/^{132}Xe$ ratios are a result of spallation by cosmic rays during Shergotty's transit from Mars to Earth. Thus, the $^{124}Xe/^{132}Xe$ traces the presence of spallation target elements (barium, light rare earth elements) in the mineral being degassed and allows releases from their major component minerals of Shergotty to be identified. The whole-rock data reveal a correlation between elevated $^{129}Xe/^{132}Xe$ and elevated $^{124}Xe/^{132}Xe$, showing that the host phase of the martian atmosphere is relatively rich in Ba and LREEs.

Figure 3b shows data from the mineral separates of the $^{129}Xe/^{132}Xe$ ratio versus the $^{124}Xe/^{132}Xe$ ratio on the same plot for comparison with the whole rock releases of Fig. 3a. Three regions are defined by the three different mineral separates. The pyroxene-dominated data shows on average a low $^{124}Xe/^{132}Xe$ ratio, which is indicative of the absence of spallation target elements. The correlation between spallation and $^{129}Xe_{xs}$ for the opaques and maskelynite grains shows a positive slope. The whole rock trend line from Fig. 3a has also been plotted for comparison and shows that the maskelynite-dominated separate's signature dominates the atmospheric xenon of the whole rock.

The evolutions of the $^{129}Xe/^{132}Xe$ ratio with cumulative ^{132}Xe release for the individual mineral separates are plotted in Fig. 4. Both the opaque-dominated (Fig. 4a) and maskelynite-dominated separates (Fig. 4b) show increasing $^{129}Xe_{xs}$ with increasing release steps, with the opaque-dominated separates being more gas-rich. The variation in $^{129}Xe_{xs}$ with release steps could be accounted for if the different minerals present (magnetite, ilmenite, and pyrrhotite) had different xenon isotopic signatures and released gas at different temperatures. However, no such explanation can account for the similar evolution of the maskelynite-dominated separates observed during analysis, since even the removal of the phosphate by the acid treatment (Msk-HCl), which left the separates essentially pure, showed no effect on the data. The pyroxene-dominated mineral separates show a consistent low $^{129}Xe/^{132}Xe$ ratio of ~1.2 over all temperature steps (Fig. 4c), except for the first steps in which a ratio close to that of the Earth's atmosphere, which we attributed to a release of adsorbed xenon, is observed. Further division of the pyroxenes into augite and pigeonite show no distinguishable differences in this ratio.

The consistently low $^{129}Xe_{xs}$ in the pyroxene-dominated data indicate that the bulk xenon component is not dominated by the martian atmospheric component as in the opaque-dominated and maskelynite-dominated mineral separates. To further understand this component the pyroxene-dominated

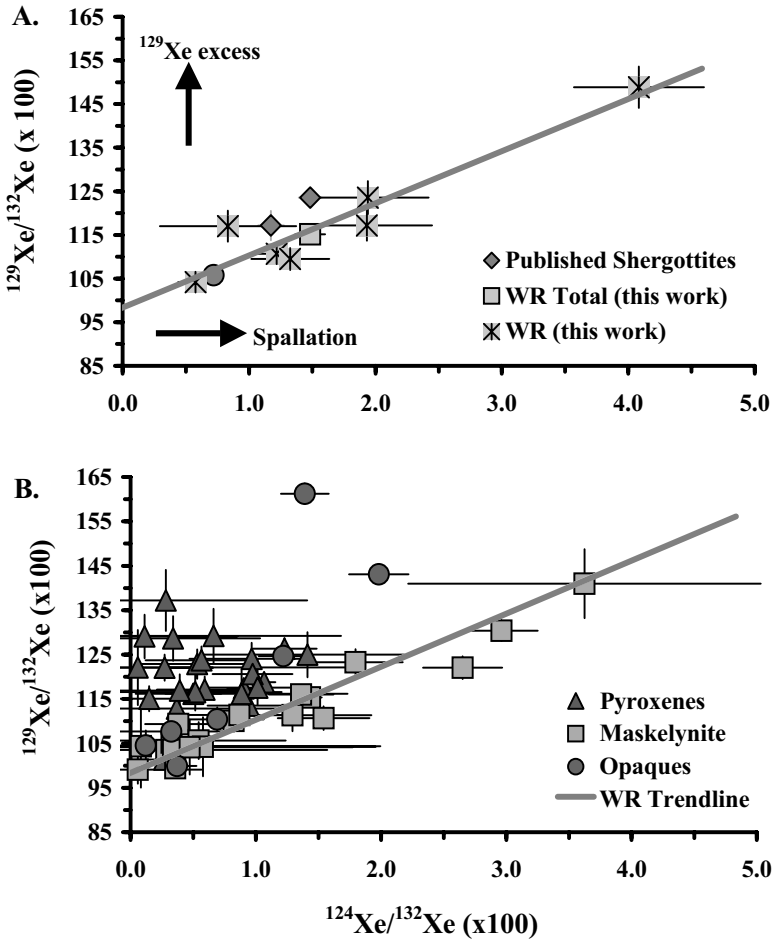

Fig. 3. The $^{129}Xe/^{132}Xe$ ratio versus the $^{124}Xe/^{132}Xe$ ratio plot of published whole rock data (Swindle et al. 1986; Ott 1988; Terribilini 2000; Mathew and Marti 2001). The whole rock observed in this experiment defines a trend line that is illustrated in plots A and B. In plot B, the pyroxene-dominated mineral separates reflect a low $^{124}Xe/^{132}Xe$ ratio due to the lack of target elements for spallation. The opaque-dominated mineral separates show a steep, positive correlation between spallation and excess $^{129}Xe/^{132}Xe$, representing a concentration of atmospheric xenon in the opaque grains. The maskelynite-dominated correlation illustrates that maskelynite grains define the whole rock trend.

data were corrected for a small spallation contribution so that they could be compared to predicted isotopic variations if the elevated $^{136}Xe/^{132}Xe$ ratio is due to fractionation or addition of fission xenon. Using the $^{124}Xe/^{132}Xe$ ratio from each release, ^{132}Xe was partitioned between a spallation component with $^{124}Xe/^{132}Xe = 0.664 \pm 0.023$ (calculated from the proportion of Ba and LREE expected for Shergotty [Lodders 1998] and using the spallation components of Hohenberg et al. [1981]) and a trapped component with $^{124}Xe/^{132}Xe = 0.0043 \pm 0.0005$ (the value and errors being chosen to encompass both solar and martian atmospheric values of this ratio). ^{129}Xe was then corrected in proportion to the calculated concentration of spallation ^{132}Xe and summed over the high temperature steps (Table 2). The near-absence of spallation in the pyroxene analyses rendered all corrections minor.

The comparison with spallation corrected data is made in Fig. 5. The trend obtained by adding fission-xenon to Chassigny solar xenon is illustrated along with the average of spallation corrected pyroxene data. Fractionation of the interior xenon gives a ratio similar to martian or terrestrial atmospheric xenon as shown in the two-component mixing line of martian interior (Chassigny solar xenon) to martian atmosphere (SPB), with further fractionation resulting in Earth's atmosphere. The pyroxene data, at better than 2σ, is consistent with a martian interior component (solar plus fission) and rules out terrestrial contamination.

DISCUSSION

By analyzing mineral separates, we have been able to identify two martian components that can be associated with identifiable mineral hosts.

The martian atmosphere component is more concentrated in the opaque-dominated mineral separates than in the maskelynite-dominated mineral separates, and is more concentrated in both than in the pyroxene-dominated. This is

Table 1. Data from Shergotty samples. ^{132}Xe in 10^{-12} cm^3 STP g^{-1}, Ratios to $^{132}Xe = 100$.

WR, bulk sample, 4.19 mg.									
1	0.189 ± 0.007	0.83 ± 0.54	1.34 ± 0.54	8.25 ± 0.74	117.01 ± 3.54	13.85 ± 0.92	81.31 ± 2.72	38.24 ± 1.65	34.89 ± 1.53
2	0.524 ± 0.010	1.22 ± 0.18	1.74 ± 0.19	9.40 ± 0.37	110.70 ± 1.71	15.50 ± 0.48	80.83 ± 1.35	38.29 ± 0.82	33.17 ± 0.74
3	0.216 ± 0.008	1.93 ± 0.51	3.50 ± 0.53	11.49 ± 0.80	117.17 ± 3.49	16.43 ± 0.96	85.05 ± 2.75	39.61 ± 1.64	32.86 ± 1.46
4	0.309 ± 0.011	4.08 ± 0.51	7.15 ± 0.59	14.22 ± 0.92	148.86 ± 4.72	17.92 ± 1.12	92.07 ± 3.33	39.36 ± 1.91	33.52 ± 1.72
5	0.422 ± 0.012	1.33 ± 0.31	1.51 ± 0.31	8.82 ± 0.53	109.47 ± 2.49	16.15 ± 0.71	80.49 ± 2.00	38.69 ± 1.22	33.31 ± 1.11
6	0.206 ± 0.008	1.94 ± 0.48	3.63 ± 0.50	11.08 ± 0.80	123.55 ± 3.79	16.07 ± 0.99	82.85 ± 2.84	38.81 ± 1.70	31.36 ± 1.49
7	0.628 ± 0.011	0.58 ± 0.14	1.01 ± 0.14	7.63 ± 0.30	104.21 ± 1.47	14.69 ± 0.42	78.76 ± 1.20	38.79 ± 0.74	33.15 ± 0.66
Total:	2.494 ± 0.026	1.48 ± 0.12	2.39 ± 0.12	9.61 ± 0.21	115.16 ± 0.98	15.68 ± 0.27	82.05 ± 0.76	38.76 ± 0.46	33.18 ± 0.42
MSK-01, maskelynite-dominated mineral separates, 7.28 mg.									
1	1.117 ± 0.011	0.36 ± 0.05	0.36 ± 0.05	7.76 ± 0.16	99.42 ± 0.77	14.60 ± 0.22	78.79 ± 0.64	39.27 ± 0.40	33.51 ± 0.36
2	0.191 ± 0.005	0.28 ± 0.29	0.26 ± 0.29	9.71 ± 0.51	103.49 ± 2.23	15.09 ± 0.64	80.48 ± 1.85	40.32 ± 1.15	34.00 ± 1.02
3	0.166 ± 0.006	0.06 ± 0.51	0.27 ± 0.51	9.67 ± 0.75	99.12 ± 3.17	14.44 ± 0.92	76.36 ± 2.62	38.27 ± 1.64	33.40 ± 1.50
4	0.374 ± 0.009	0.33 ± 0.26	0.60 ± 0.26	9.24 ± 0.46	105.17 ± 2.07	15.19 ± 0.59	79.37 ± 1.68	39.61 ± 1.05	34.08 ± 0.95
5	0.212 ± 0.005	0.38 ± 0.27	0.66 ± 0.27	7.53 ± 0.44	109.37 ± 2.20	14.80 ± 0.60	81.22 ± 1.76	40.03 ± 1.08	33.60 ± 0.97
6	0.774 ± 0.009	0.82 ± 0.08	1.15 ± 0.08	8.47 ± 0.20	110.06 ± 0.99	15.51 ± 0.28	80.17 ± 0.78	38.94 ± 0.48	33.52 ± 0.43
7	0.089 ± 0.004	0.54 ± 0.70	0.84 ± 0.70	8.74 ± 0.92	105.63 ± 4.16	14.41 ± 1.16	80.44 ± 3.41	37.81 ± 2.06	33.42 ± 1.88
8	0.147 ± 0.005	0.87 ± 0.46	1.54 ± 0.46	9.05 ± 0.69	111.41 ± 3.11	15.38 ± 0.87	82.76 ± 2.51	40.11 ± 1.52	33.00 ± 1.36
9	0.734 ± 0.008	1.43 ± 0.09	1.93 ± 0.10	9.33 ± 0.21	115.35 ± 1.02	16.05 ± 0.28	81.81 ± 0.79	39.09 ± 0.47	33.23 ± 0.42
10	0.189 ± 0.004	1.36 ± 0.26	2.50 ± 0.28	10.04 ± 0.47	115.99 ± 2.20	16.33 ± 0.60	82.93 ± 1.71	39.42 ± 1.03	33.75 ± 0.92
11	0.170 ± 0.004	2.65 ± 0.32	3.49 ± 0.34	12.25 ± 0.57	122.06 ± 2.55	16.82 ± 0.68	83.65 ± 1.92	39.51 ± 1.15	34.03 ± 1.04
12	0.288 ± 0.006	2.96 ± 0.29	4.05 ± 0.31	12.33 ± 0.50	130.40 ± 2.34	17.38 ± 0.61	85.06 ± 1.71	38.99 ± 1.01	33.33 ± 0.91
13	0.379 ± 0.011	1.80 ± 0.38	2.49 ± 0.39	12.48 ± 0.65	123.29 ± 2.91	17.01 ± 0.78	84.43 ± 2.21	38.72 ± 1.30	32.36 ± 1.16
Total:	4.831 ± 0.025	1.00 ± 0.06	1.40 ± 0.06	9.33 ± 0.11	110.45 ± 0.48	15.58 ± 0.13	80.95 ± 0.38	39.21 ± 0.23	33.45 ± 0.21
MSK-02, maskelynite-dominated mineral separates, 1.59 mg.									
1	0.478 ± 0.015	0.11 ± 0.45	−0.20 ± 0.45	6.81 ± 0.61	97.07 ± 2.72	14.84 ± 0.81	78.47 ± 2.32	38.60 ± 1.42	32.51 ± 1.29
2	0.701 ± 0.021	1.73 ± 0.42	3.00 ± 0.44	11.44 ± 0.69	147.11 ± 3.49	16.83 ± 0.82	82.19 ± 2.28	39.77 ± 1.38	32.28 ± 1.23
3	0.664 ± 0.022	4.55 ± 0.52	5.38 ± 0.55	15.02 ± 0.84	161.52 ± 4.10	18.73 ± 0.94	88.07 ± 2.61	39.26 ± 1.51	33.68 ± 1.38
4	0.414 ± 0.015	7.09 ± 0.81	12.74 ± 0.97	25.22 ± 1.40	180.65 ± 6.02	26.29 ± 1.46	99.10 ± 3.80	35.50 ± 1.98	32.54 ± 1.85
Total:	2.257 ± 0.037	3.15 ± 0.26	4.71 ± 0.28	13.90 ± 0.42	146.43 ± 1.97	18.60 ± 0.48	86.07 ± 1.33	38.63 ± 0.78	32.79 ± 0.71
MSK-HCL, acid washed maskelynite mineral separates, 1.33 mg.									
1	0.225 ± 0.014	0.58 ± 1.38	0.48 ± 1.38	7.59 ± 1.54	104.23 ± 6.67	15.53 ± 1.94	79.17 ± 5.50	42.79 ± 3.52	33.51 ± 3.19
2	0.222 ± 0.013	0.34 ± 1.23	−0.14 ± 1.23	8.67 ± 1.44	103.55 ± 6.06	15.26 ± 1.76	77.98 ± 4.98	40.10 ± 3.13	31.76 ± 2.85
3	0.171 ± 0.015	0.08 ± 1.91	0.58 ± 1.91	7.03 ± 2.11	104.34 ± 9.31	17.13 ± 2.69	77.24 ± 7.55	38.72 ± 4.79	34.50 ± 4.45
4	0.263 ± 0.016	0.47 ± 1.30	0.41 ± 1.30	7.38 ± 1.46	104.16 ± 6.18	16.78 ± 1.84	75.07 ± 4.97	37.58 ± 3.12	32.17 ± 2.91
5	0.387 ± 0.015	1.29 ± 0.63	1.31 ± 0.63	8.00 ± 0.81	111.37 ± 3.63	16.15 ± 1.02	82.25 ± 2.93	39.90 ± 1.79	34.20 ± 1.64
6	0.547 ± 0.016	1.54 ± 0.37	1.70 ± 0.37	9.86 ± 0.59	110.70 ± 2.67	16.48 ± 0.76	82.78 ± 2.15	39.26 ± 1.29	34.98 ± 1.20
7	0.308 ± 0.019	3.62 ± 1.41	5.31 ± 1.43	19.28 ± 1.96	140.99 ± 7.78	19.02 ± 2.03	93.74 ± 5.77	37.24 ± 3.25	32.05 ± 3.00
8	0.554 ± 0.025	6.08 ± 0.96	8.92 ± 1.05	18.89 ± 1.42	139.91 ± 5.61	23.30 ± 1.60	96.26 ± 4.24	37.38 ± 2.32	30.70 ± 2.10
Total:	2.676 ± 0.048	2.27 ± 0.35	3.04 ± 0.36	11.72 ± 0.46	117.84 ± 1.91	17.95 ± 0.55	84.84 ± 1.51	38.92 ± 0.90	33.00 ± 0.83

Table 1. *Continued.* Data from Shergotty samples. ^{132}Xe in 10^{-12} cm^3 STP g^{-1}, Ratios to $^{132}Xe = 100$.

OPQ-01, opaque-dominated mineral separates, 1.06 mg.									
1	2.032 ± 0.036	0.37 ± 0.16	0.38 ± 0.16	7.07 ± 0.33	99.92 ± 1.47	14.83 ± 0.43	79.93 ± 1.24	39.27 ± 0.76	34.55 ± 0.70
2	0.617 ± 0.023	0.12 ± 0.54	0.32 ± 0.54	5.71 ± 0.79	104.54 ± 3.38	14.05 ± 0.95	80.14 ± 2.77	40.54 ± 1.73	33.76 ± 1.54
3	0.550 ± 0.020	0.33 ± 0.50	0.20 ± 0.50	6.51 ± 0.76	107.67 ± 3.31	13.67 ± 0.90	79.23 ± 2.64	39.66 ± 1.63	33.53 ± 1.47
4	0.865 ± 0.026	0.69 ± 0.37	0.66 ± 0.37	7.20 ± 0.62	110.42 ± 2.73	14.39 ± 0.75	81.11 ± 2.17	41.00 ± 1.35	33.50 ± 1.19
5	1.750 ± 0.035	1.22 ± 0.20	1.43 ± 0.20	8.64 ± 0.41	124.68 ± 1.96	15.24 ± 0.50	80.53 ± 1.42	39.59 ± 0.87	34.48 ± 0.79
6	1.899 ± 0.039	1.98 ± 0.24	3.01 ± 0.26	10.33 ± 0.46	143.10 ± 2.26	15.88 ± 0.53	84.76 ± 1.52	39.83 ± 0.91	34.26 ± 0.82
7	2.439 ± 0.048	1.39 ± 0.19	2.25 ± 0.21	9.79 ± 0.41	161.22 ± 2.33	15.84 ± 0.50	82.52 ± 1.41	39.71 ± 0.85	33.94 ± 0.77
Total:	10.510 ± 0.089	1.07 ± 0.09	1.51 ± 0.10	8.50 ± 0.18	128.41 ± 0.89	15.18 ± 0.22	81.62 ± 0.63	39.78 ± 0.38	34.14 ± 0.35
PYX-01, pyroxene-dominated mineral separates, 7.84 mg.									
1	0.103 ± 0.003	0.15 ± 0.36	0.76 ± 0.36	12.45 ± 0.68	115.06 ± 2.84	14.26 ± 0.74	76.55 ± 2.11	40.05 ± 1.35	35.27 ± 1.24
2	0.165 ± 0.005	0.27 ± 0.39	0.45 ± 0.39	8.56 ± 0.61	122.05 ± 2.94	14.20 ± 0.76	78.96 ± 2.16	40.90 ± 1.36	34.07 ± 1.22
3	0.188 ± 0.004	0.50 ± 0.22	0.66 ± 0.22	7.45 ± 0.40	116.19 ± 2.06	14.72 ± 0.55	80.67 ± 1.58	41.11 ± 0.99	34.16 ± 0.88
4	0.045 ± 0.002	0.37 ± 0.81	0.51 ± 0.81	5.88 ± 1.01	112.83 ± 4.92	13.34 ± 1.32	79.81 ± 3.86	39.98 ± 2.40	33.52 ± 2.15
5	0.552 ± 0.008	1.07 ± 0.09	1.40 ± 0.10	8.79 ± 0.24	118.76 ± 1.25	15.88 ± 0.33	81.26 ± 0.94	39.30 ± 0.58	33.54 ± 0.52
6	0.094 ± 0.008	0.94 ± 0.33	1.51 ± 0.33	9.31 ± 0.56	113.53 ± 2.61	15.72 ± 0.72	81.33 ± 2.04	41.05 ± 1.27	32.87 ± 1.11
7	0.159 ± 0.005	0.59 ± 0.38	1.12 ± 0.38	9.11 ± 0.62	117.14 ± 2.92	16.33 ± 0.81	80.24 ± 2.23	38.50 ± 1.35	33.58 ± 1.24
8	0.432 ± 0.008	0.90 ± 0.13	1.18 ± 0.14	9.16 ± 0.33	117.39 ± 1.62	15.31 ± 0.43	79.87 ± 1.21	39.77 ± 0.75	33.26 ± 0.67
Total:	1.738 ± 0.016	0.78 ± 0.08	1.11 ± 0.08	8.92 ± 0.15	117.49 ± 0.76	15.35 ± 0.20	80.27 ± 0.57	39.86 ± 0.35	33.63 ± 0.32
PYX-02, pyroxene-dominated mineral separates, 6.25 mg.									
1	0.573 ± 0.009	0.27 ± 0.13	1.35 ± 0.14	52.39 ± 0.82	101.35 ± 1.35	16.18 ± 0.41	76.41 ± 1.10	37.87 ± 0.68	30.96 ± 0.60
2	0.099 ± 0.004	0.11 ± 0.74	0.79 ± 0.74	7.25 ± 1.09	129.08 ± 4.93	12.69 ± 1.18	79.96 ± 3.50	39.82 ± 2.17	34.79 ± 1.98
3	0.122 ± 0.004	0.53 ± 0.44	1.00 ± 0.45	7.79 ± 0.73	122.88 ± 3.31	14.73 ± 0.85	81.21 ± 2.45	39.67 ± 1.50	34.31 ± 1.36
4	0.102 ± 0.004	0.97 ± 0.50	2.37 ± 0.50	7.70 ± 0.79	124.06 ± 3.60	14.26 ± 0.91	81.77 ± 2.66	39.74 ± 1.62	34.33 ± 1.47
5	0.193 ± 0.005	0.97 ± 0.32	1.61 ± 0.32	7.39 ± 0.55	120.63 ± 2.61	14.14 ± 0.66	82.00 ± 1.97	40.15 ± 1.20	33.65 ± 1.08
6	0.263 ± 0.006	1.23 ± 0.26	1.44 ± 0.26	7.95 ± 0.48	126.35 ± 2.35	15.50 ± 0.60	81.04 ± 1.69	40.52 ± 1.05	34.68 ± 0.95
7	0.111 ± 0.005	0.52 ± 0.69	0.53 ± 0.69	6.96 ± 0.97	116.58 ± 4.16	13.83 ± 1.10	77.94 ± 3.12	40.93 ± 1.98	33.36 ± 1.76
8	0.266 ± 0.008	0.57 ± 0.45	1.08 ± 0.45	6.29 ± 0.67	123.74 ± 3.11	14.83 ± 0.81	81.26 ± 2.30	41.24 ± 1.43	34.74 ± 1.28
Total:	1.730 ± 0.017	0.60 ± 0.12	1.30 ± 0.12	22.33 ± 0.31	116.07 ± 0.94	15.07 ± 0.25	79.41 ± 0.71	39.58 ± 0.44	33.20 ± 0.39
PYX-03, pyroxene-dominated mineral separates, 2.45 mg.									
1	0.081 ± 0.006	0.06 ± 1.74	−0.32 ± 1.74	7.05 ± 1.92	122.09 ± 8.46	11.86 ± 2.15	77.97 ± 6.25	39.76 ± 3.91	35.62 ± 3.62
2	0.321 ± 0.012	0.39 ± 0.51	0.24 ± 0.51	0.97 ± 0.84	116.89 ± 3.66	12.96 ± 0.95	81.64 ± 2.83	39.59 ± 1.73	36.12 ± 1.60
3	0.498 ± 0.020	1.01 ± 0.40	1.48 ± 0.40	8.60 ± 0.78	117.54 ± 3.92	14.13 ± 1.01	82.07 ± 3.04	39.39 ± 1.86	33.48 ± 1.68
4	0.214 ± 0.011	0.89 ± 0.85	0.42 ± 0.85	7.58 ± 1.13	116.20 ± 5.57	14.72 ± 1.47	80.71 ± 4.30	40.52 ± 2.70	33.12 ± 2.40
5	0.278 ± 0.012	0.34 ± 0.70	0.20 ± 0.70	7.22 ± 0.96	128.64 ± 5.01	15.16 ± 1.24	80.90 ± 3.63	38.87 ± 2.23	35.09 ± 2.05
Total	1.392 ± 0.029	0.65 ± 0.29	0.64 ± 0.29	6.21 ± 0.44	119.62 ± 2.14	14.01 ± 0.55	81.25 ± 1.63	39.55 ± 1.01	34.51 ± 0.92
AUG, augite-dominated mineral separates, 1.55 mg.									
1	0.065 ± 0.009	2.05 ± 2.37	2.56 ± 2.37	14.58 ± 2.81	126.71 ± 11.58	12.36 ± 2.90	81.45 ± 8.50	42.08 ± 5.36	35.57 ± 4.81
2	0.396 ± 0.017	1.41 ± 0.83	1.97 ± 0.83	8.68 ± 1.04	124.98 ± 5.06	15.88 ± 1.31	81.76 ± 3.76	37.82 ± 2.26	32.52 ± 2.03
3	0.244 ± 0.012	0.66 ± 1.02	2.77 ± 1.02	10.59 ± 1.31	129.23 ± 6.07	15.76 ± 1.53	80.79 ± 4.39	38.90 ± 2.69	33.77 ± 2.42
4	0.197 ± 0.011	0.28 ± 1.13	1.17 ± 1.13	7.83 ± 1.32	137.20 ± 6.87	12.31 ± 1.54	79.95 ± 4.74	38.83 ± 2.92	34.77 ± 2.66
Total:	0.902 ± 0.026	1.05 ± 0.57	2.07 ± 0.57	9.72 ± 0.70	128.95 ± 3.30	14.63 ± 0.82	81.07 ± 2.39	38.85 ± 1.46	33.71 ± 1.32

Table 1. *Continued.* Data from Shergotty samples. ^{132}Xe in 10^{-12} cm^3 STP g^{-1}, Ratios to $^{132}Xe = 100$.

PIG, pigeonite-dominated mineral separates, 1.51 mg.									
1	0.260 ± 0.016	0.35 ± 1.23	1.26 ± 1.23	8.36 ± 2.05	124.06 ± 6.71	17.45 ± 1.92	78.45 ± 4.87	43.51 ± 3.20	35.64 ± 2.78
2	0.263 ± 0.011	1.31 ± 0.77	1.50 ± 0.77	8.34 ± 0.95	125.41 ± 4.32	15.04 ± 1.10	84.05 ± 3.21	38.06 ± 1.92	33.96 ± 1.75
3	0.237 ± 0.011	1.37 ± 0.94	2.14 ± 0.94	10.29 ± 1.17	120.36 ± 4.79	17.18 ± 1.34	81.20 ± 3.60	36.82 ± 2.17	33.44 ± 1.99
4	0.279 ± 0.013	1.36 ± 0.87	1.55 ± 0.88	8.53 ± 1.21	118.76 ± 4.89	16.61 ± 1.35	83.93 ± 3.80	40.07 ± 2.30	33.10 ± 2.06
5	0.303 ± 0.014	1.19 ± 0.89	2.10 ± 0.90	7.80 ± 1.20	127.32 ± 5.20	16.03 ± 1.36	83.74 ± 3.84	38.39 ± 2.28	32.16 ± 2.07
6	0.241 ± 0.013	0.20 ± 1.04	3.24 ± 1.07	9.45 ± 1.43	142.46 ± 6.36	13.10 ± 1.44	81.11 ± 4.26	40.76 ± 2.65	32.69 ± 2.36
Total:	1.583 ± 0.032	0.98 ± 0.39	1.97 ± 0.39	8.76 ± 0.55	126.42 ± 2.19	15.86 ± 0.58	82.22 ± 1.61	39.55 ± 0.99	33.44 ± 0.88

Table 2. Spallation-corrected xenon. Concentrations in 10^{-12} cm^3 STP g^{-1}.

	$^{132}Xe_{total}$	$^{129}Xe/^{132}Xe$	$^{129}Xe_{xs}$	$^{132}Xe_{interior}$
WR (bulk sample, 4.19 mg)	2.494 ± 0.026	1.153 ± 0.011	0.311 ± 0.007	2.291 ± 0.213
MSK-01 (maskelynite-dominated mineral separates, 7.28 mg)	4.831 ± 0.025	1.105 ± 0.007	0.353 ± 0.007	4.405 ± 0.203
MSK-02 (maskelynite-dominated mineral separates, 1.59 mg)	2.257 ± 0.037	1.473 ± 0.021	0.931 ± 0.024	1.421 ± 0.291
MSK-HCL (acid washed maskelynite mineral separates, 1.33 mg)	2.676 ± 0.048	1.180 ± 0.020	0.393 ± 0.012	2.309 ± 0.494
OPQ-01 (opaque-dominated mineral separates, 1.06 mg)	10.150 ± 0.089	1.285 ± 0.010	2.617 ± 0.056	8.315 ± 0.712
PYX-01 (pyroxene-dominated mineral separates, 7.84 mg)	1.738 ± 0.016	1.175 ± 0.008	0.269 ± 0.005	1.650 ± 0.111
PYX-02 (pyroxene-dominated mineral separates, 6.25 mg)	1.730 ± 0.017	1.161 ± 0.009	0.231 ± 0.005	1.584 ± 0.133
PYX-03 (pyroxene-dominated mineral separates, 2.45 mg)	1.393 ± 0.029	1.196 ± 0.021	0.219 ± 0.006	1.153 ± 0.261
AUG (augite-dominated mineral separates, 1.55 mg)	0.902 ± 0.026	1.290 ± 0.033	0.252 ± 0.009	0.783 ± 0.313
PIG (pigeonite-dominated mineral separates, 1.51 mg)	1.583 ± 0.032	1.264 ± 0.022	0.385 ± 0.011	1.358 ± 0.347

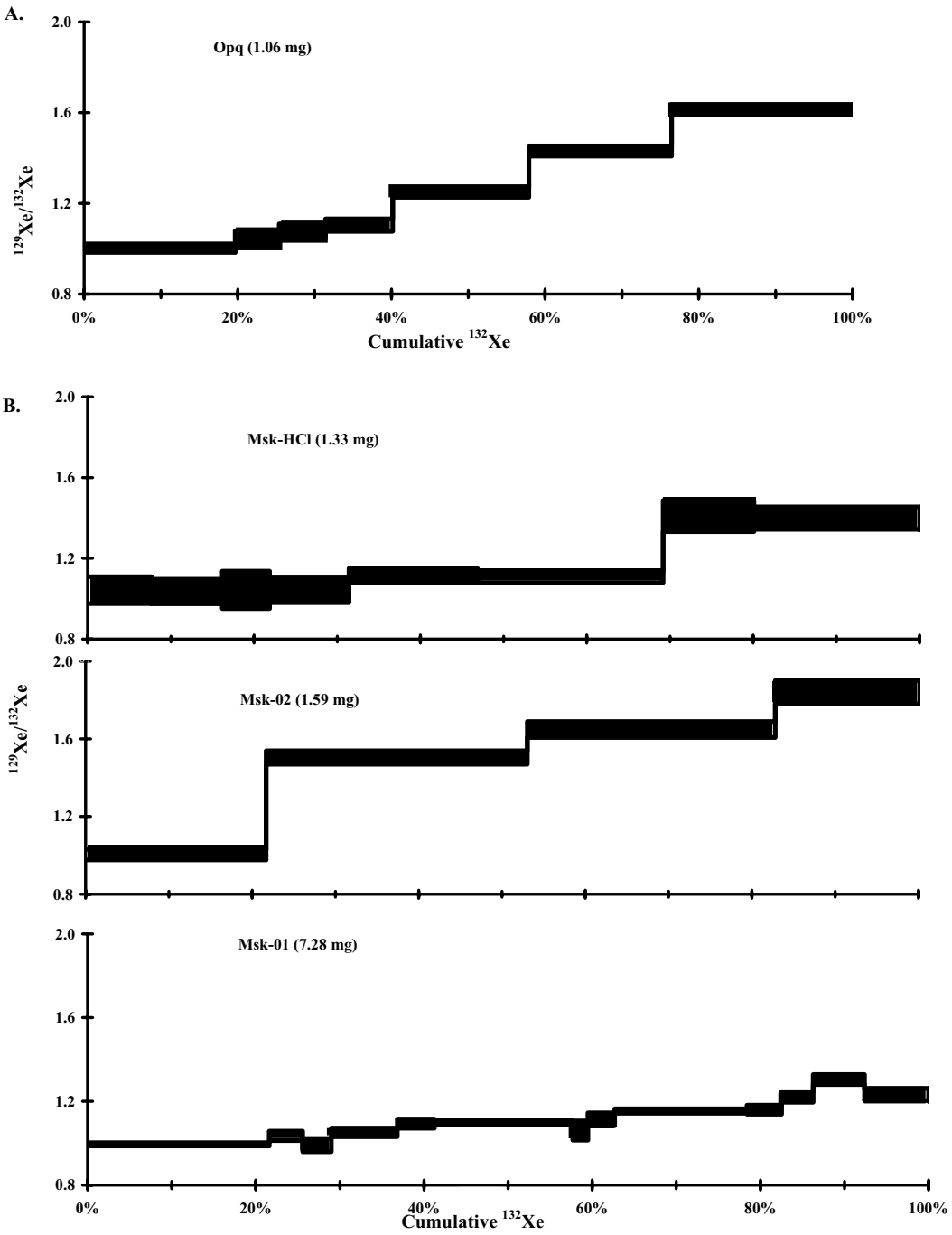

Fig. 4. The evolutions of the $^{129}Xe/^{132}Xe$ ratio with temperatures for the individual mineral separates: opaques (a), maskelynite (b). The opaques and maskelynite show an increase in excess $^{129}Xe/^{132}Xe$ (the opaques are more gas-rich), while the pyroxene shows a consistent $^{129}Xe/^{132}Xe = 1.2$. See text for further details.

in turn consistent with the model of shock incorporation of adsorbed atmospheric gas invoked for the nakhlites and for ALH 84001 (Gilmour et al. 1998). The smaller the grain size, the more surface area per unit mass is available to atmospheric gas, resulting in higher concentrations of xenon after shock incorporation. From our mineral separates, the smallest grain sizes are the opaques (<400 μm), followed by the maskelynite (~1 mm), and finally the pyroxenes (>3 mm). This broadly corresponds to the trend in atmospheric concentration observed in the mineral separates that the opaque-dominated separates have a higher gas concentration followed by maskelynite-dominated separates, and lastly the pyroxene-dominated mineral separates. Shock implantation of adsorbed atmospheric gas seems to be the most viable

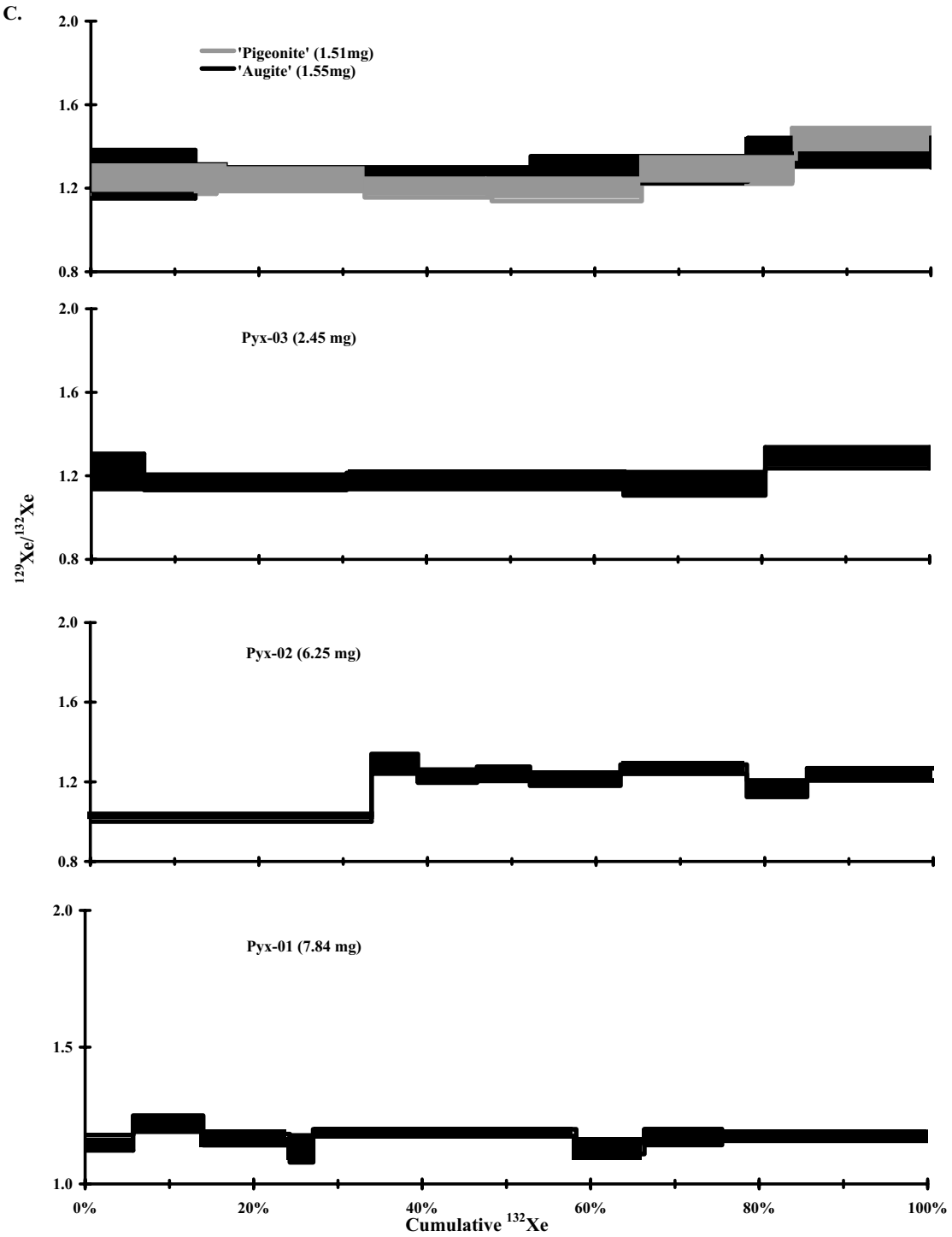

Fig. 4. *Continued.* The evolutions of the $^{129}Xe/^{132}Xe$ ratio with temperatures for the individual mineral separates: pyroxene (c). The opaques and maskelynite show an increase in excess $^{129}Xe/^{132}Xe$ (the opaques are more gas-rich), while the pyroxene shows a consistent $^{129}Xe/^{132}Xe$ 1.2. See text for further details.

explanation of the observed gas concentration in the mineral separates. Were shock implantation alone responsible, we might expect that maskelynite-dominated separates, a short-term order crystalline mineral formed from plagioclase that has experienced shock, would have higher emplacement of gases than the opaque-dominated separates.

The process that led to the incorporation of xenon from the martian atmosphere is also implicated in the elemental

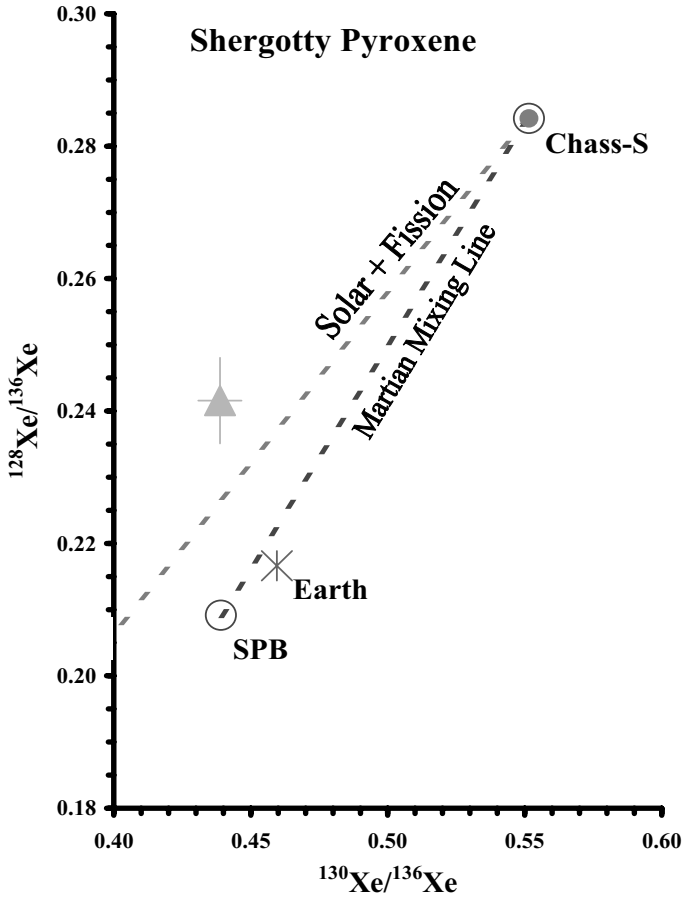

Fig. 5. A $^{128}Xe/^{136}Xe$ versus $^{130}Xe/^{136}Xe$ graph of the average of spallation corrected pyroxene data; errors are 1σ. The component defined by the pyroxene mineral separates is consistent with having been generated by the addition of fission-xenon to solar xenon and is thus similar to the interior components measured in Chassigny. The data point is not consistent with terrestrial contamination.

fractionation that decreased the Kr/Xe ratio observed in the martian meteorites. Reports (Drake et al. 1994; Musselwhite and Swindle 2001) suggest that the shergottites define an array that is broadly consistent with mixing between a martian atmosphere-like component and a martian mantle-like component. The nakhlite and shergottite heavy noble gas data are in fact both consistent with the atmosphere's elemental composition (Musselwhite and Swindle 2001), though other elements suggest the shergottite component is closer to the true atmospheric value. The nakhlites and ALH 84001 have a lower $^{84}Kr/^{132}Xe$ ratio for their high $^{129}Xe/^{132}Xe$ ratio than can be consistent with the same simple mixing array of the shergottites (Fig. 6). Studies of the nakhlites and ALH 84001 led to the suggestion that the Kr/Xe ratio observed is due to an elemental fractionation of the atmospheric reservoir during the adsorption of atmospheric gases onto mineral surfaces, followed by shock implantation (Gilmour et al. 2001).

Adsorption of xenon on mineral surfaces is significant at the temperatures characteristic of the martian surface. Adsorption studies (Fanale et al. 1978) show that at partial pressures above 10^{-2} Torr, xenon and krypton adsorption on basalt follows a semi-empirical Freundlich relationship (Freundlich 1930, cited in Fanale et al.). Extrapolating this to partial pressures characteristic of the martian surface is problematic, and two approaches were taken that plausibly lead to bracketing the true value. A maximum adsorbed concentration is obtained if the observed correlation is assumed to hold to low pressure, while a minimum is obtained by assuming the Freundlich relationship is replaced by a Henry's law relationship below the lowest pressure for which data are available. Figure 7 illustrates the implications of these maximum and minimum adsorption efficiencies in a simple model. Separating two surfaces creates a void space in which constant partial pressures of xenon and krypton are maintained. We plot the ratio of Kr/Xe in the assembly (void space + adsorbed component on surfaces) normalized to the ratio in the ambient gas phase as a function of the distance separating the surfaces. In our model, this ensemble represents the gas available for implantation into mineral surfaces in the event of a shock. The observed depletion of the ratio represented by the nakhlites compared to the shergottites (Kr depletion factor of 0.20–0.25) is obtained with separations between 5 μm and 100 μm, depending on the details of adsorption at low pressures. This implies that some

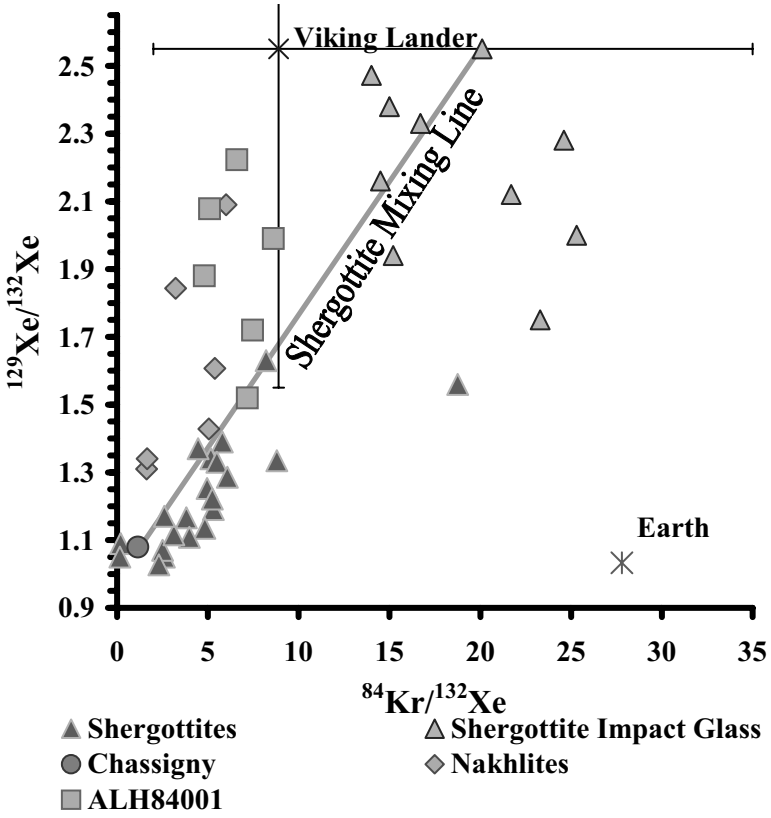

Fig. 6. The $^{84}Kr/^{132}Xe$ versus $^{129}Xe/^{132}Xe$ ratio for some SNC meteorites. Most shergottites define a mixing between martian interior (Chassigny) and martian atmosphere (EET 79001-Glass) as seen in this graph. Falling off this mixing line are the nakhlites and ALH 84001 due to mass fractionation or the possible existence of a third high $^{129}Xe/^{132}Xe$ reservoir (see text for further discussion). Impact glass shows a mixing of a component identified in crushed samples that yield a low $^{129}Xe/^{132}Xe$ ratio (Ott 1988). Data is from literature (Owen et al. 1977; Ozima and Podosek 1983; Becker and Pepin 1984; Bogard et al. 1984; Swindle et al. 1986; Ott 1988; Ott et al. 1988; Wiens 1988; Swindle et al. 1989; Ott and Lohr 1992; Drake et al. 1994; Miura et al. 1995; Swindle et al. 1995; Murty and Mohapatra 1997; Bogard and Garrison 1998; Garrison and Bogard 2000; Mohapatra and Ott 2000; Swindle et al. 2000; Terribilini 2000; Bart et al. 2001).

degree of elemental fractionation enhancing Xe in the trapped component is to be expected, and re-emphasizes that trapping without fractionation is the exception rather than the rule.

It is interesting to note that the measurement of Lithology C of the shergottite Elephant Moraine (EET) A79001 (Bogard and Johnson 1983; Becker and Pepin 1984; Bogard et al. 1984) and later calculated as SPB (Swindle et al. 1986) is at one extreme of the proposed shergottite mixing array, while whole rock (dominated by pyroxene) analyses have uniformly low $^{129}Xe/^{132}Xe$ and Kr/Xe ratios close to that of Chassigny. However, given that whole rock Shergotty data is not a mixture of an atmospheric shock glass component and an interior component, it is not clear in Fig. 6 whether it properly belongs with the shergottite glass-mixing array or with the nakhlites-mixing array. It is accepted that the shergottite glass acquired its budget of martian atmospheric gases as a result of shock trapping, and that shock can result in the trapping of ambient gases without elemental fractionation (Bogard et al. 1986; Wiens and Pepin 1986). We propose that the signature seen in Shergotty resulted from shock incorporation of martian atmosphere that had been adsorbed on grain surfaces (and hence elementally fractionated) as explained in the fractionated components of ALH 84001 (Gilmour et al. 1998), Nakhla (Gilmour et al. 1999; Gilmour et al. 2001), and in iddingsite from Lafayette (Swindle et al. 2000).

The consistent $^{129}Xe/^{132}Xe$ ratio observed in the pyroxene-dominated mineral separates (Fig. 4) suggests a single component is present that is consistent with mixing of solar and fission xenon (Fig. 6). In contrast, other separates exhibit releases with higher and lower $^{129}Xe/^{132}Xe$ ratios, possibly because these finer-grained separates were more susceptible to both air contamination and shock incorporation of martian atmosphere. The pyroxene signature is similar to the other documented martian interior components, such as those observed in ALH 84001 and Chass-E (Mathew and Marti 2001). The uniformity of the mixture in the pyroxene-dominated mineral separates suggests that this is the signature of the ambient xenon present in the magma from which they crystallized, and notably that this is an elevated $^{129}Xe/^{132}Xe$ ratio. It remains unclear whether the elevated $^{129}Xe/^{132}Xe$ ratio observed in this component is evidence of an admixture

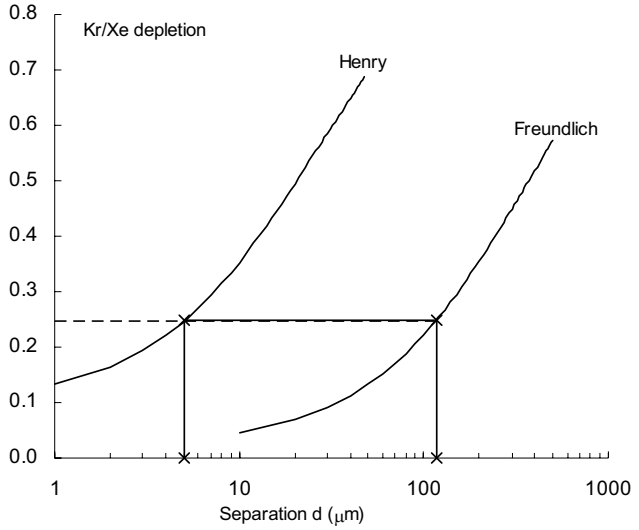

Fig. 7. In an ensemble with surfaces available for adsorption separated by a distance *d*, the ratio between the Kr/Xe ratio of the whole ensemble (adsorbed component ±ambient xenon) and the Kr/Xe ratio of the gas phase is plotted as a function of the distance *d*. Following Fanale et al. (1978) adsorption efficiencies are estimated using the Freundlich relationship and Henry's Law relationship, resulting in two relationships. The Kr depletion factor of the nakhlites is used to estimate the maximum and minimum separation of the surfaces responsible.

of martian atmosphere to the melt perhaps consistent with the high crustal contribution, or if the elevated $^{129}Xe/^{132}Xe$ is preserved in the source region of the interior component.

However, the preservation of a fission anomaly from ^{244}Pu in the young meteorites suggests degassing that ceased early in martian history. This allowed xenon components with elevated $^{136}Xe/^{132}Xe$ ratios to form as ^{244}Pu decayed and subsequently conserve these components. For nakhlites, the interior component is preserved in the mesostasis (Gilmour et al. 1999) and hence correlates with large ion lithophiles. Marty and Marti (2002) argued that data from the nakhlites exhibit the extreme case in which xenon behaved as an incompatible element in a closed system during crystallization. They interpret the relatively low ratio of $^{136}Xe^*/Pu$ as evidence of degassing of the source region for the first 170 Ma to 330 Ma of formation and subsequent closure.

This interpretation, however, requires quantitative retention of ^{136}Xe during crystallization of the nakhlites. In this context, the absence of identifiable excesses of parentless ^{40}Ar from ^{40}K decay in the nakhlites is problematic (inherited ^{40}Ar has been identified in the shergottites [Mathew et al. 2003]). A source region with substantial fission anomalies from ^{244}Pu decay must have closed to xenon loss within 500 Ma of the origin of the solar system, suggesting that ^{40}Ar should have accumulated over ~2.7 Ga before the formation of the nakhlites. Nakhla has a well-defined ^{40}Ar-^{39}Ar age of 1.33 ± 0.03 Ga and a bulk K-Ar age of 1.36 ± 0.03 Ga (Podosek 1973). These are both identical to the accepted crystallization age of Nakhla, and indicate that the parent melt was substantially degassed of argon on or shortly before formation. Preservation of ^{136}Xe fission anomalies in the nakhlites that would allow the chronology of the source region to be inferred thus requires partition and loss of argon away from xenon at some point during or shortly before formation without significant xenon loss. Such a process is hard to envisage since argon is more soluble in silicate melts than xenon (Caroll and Webster 1994).

Another suggestion for the anomalous fission ^{136}Xe is to consider the assimilation of a crustal component in Shergotty's melt. Because of their comparable ionic radii, Pu can behave similarly to the LREE in igneous fractionation process (Shukolyukov and Begemann 1996). Thus, Pu could reside in a more evolved component, such as the martian crusts, and become assimilated into the parent melt before crystallization. This follows the similar indications of epsilon Nd and the oxygen fugacity and that Shergotty reflects a high mixing of a crustal component in its parent melt.

CONCLUSIONS

The maskelynite-dominated, opaque-dominated, and pyroxene-dominated mineral separates that were physically separated from Shergotty contain uniquely identified martian atmospheric and interior xenon components. Martian atmospheric xenon (^{129}Xe excess over $^{129}Xe/^{132}Xe$=1) is 5–10 times more concentrated in opaque-dominated separates and maskelynite-dominated than in pyroxene. Gas concentrations are argued to be related to the grain size in that the smallest grains present greater surface area for adsorption before shock incorporation of martian atmospheric xenon. This is the same mechanism said to account for the incorporation of martian atmospheric xenon in Nakhla. Thus, the measured bulk Kr/Xe ratio in the shergottites may be the same elemental fractionations between EET A79001 melt glass and nakhlites, and not always a simple mixing of martian mantle and martian atmosphere.

The interior component consists of solar xenon with a fission contribution similar to that suggested by Chass-E, although with a higher fission contribution (Mathew and Marti 2001). Though present in all minerals analyzed, it is best defined in pyroxene-dominated separates. This is consistent with its identification in high-temperature releases from whole rock analyses (Mathew and Marty 2001, 2002; Mathew et al. 2003). Pyroxene-dominated separates exhibit a consistent $^{129}Xe_{xs}$ ($^{129}Xe/^{132}Xe$ ~1.2) that contrasts with the maskelynite-dominated and opaque-dominated separates where $^{129}Xe/^{132}Xe$ increased with increasing release temperature. This interior component in pyroxene-dominated separates is thought to be ambient xenon, which is a mixture of solar, fission, and atmospheric components present in the magma in which the pyroxenes formed before incorporation. The fission contribution in the interior component is

evidence either of an admixture of martian atmosphere to the melt with a high crustal contribution or of a preservation of a fission anomaly from ^{244}Pu in the source region of the interior component. Further investigation of the interior component in the basaltic shergottites may help understand the fission contribution and its presence.

Acknowledgments–We are thankful to C. Davies, R. Lentz, and H. McSween for their support in mineral separation, identification, and discussion. The manuscript benefited from constructive reviews from D. D. Bogard and K. J. Mathew. This work was funded by the Geological Science Department, the University of Tennessee, the PPARC, and the Royal Society. The sample of Shergotty (#1985, MFH) was provided by the Natural History Museum of London, England.

REFERENCES

Bart G. D., Swindle T. D., Olson E. K., and Treiman A. H. 2001. Xenon and krypton in Nakhla mineral separates (abstract #1363). 32nd Lunar and Planetary Science Conference. CD-ROM.

Becker R. H. and Pepin R. O. 1984. The case for a martian origin of the shergottites: Nitrogen and noble gases in EET A79001. *Earth and Planetary Science Letters* 69:225–242.

Bogard D. D. and Garrison D. H. 1998. Trapped and radiogenic argon in martian shergottites (abstract). *Meteoritics & Planetary Science* 33:A19.

Bogard D. D., Horz F., and Johnson P. H. 1986. Shock-implanted noble gases—An experimental study with implications for the origin of martian gases in shergottite meteorites. *Journal of Geophysical Research* 91:E99–E114.

Bogard D. D. and Johnson P. 1983. Martian gases in an Antarctic meteorite. *Science* 221:651–654.

Bogard D. D., Nyquist L. E., and Johnson P. 1984. Noble gas contents of shergottites and implications for the martian origin of SNC meteorites. *Geochimica et Cosmochimica Acta* 48:1723–1739.

Borg L. E., Nyquist L. E., Taylor L. A., Wiesmann H., and Chi-Y S. 1997. Constraints on martian differentiation processes from Rb-Sr and Sm-Nd isotopic analyses of the basaltic shergottite QUE 94201. *Geochimica et Cosmochimica Acta* 61:4915–4931.

Chen J. H. and Wasserburg G. J. 1986. Formation ages and evolution of Shergotty and its parent planet from U-Th-Pb systematics. *Geochimica et Cosmochimica Acta* 50:955–968.

Drake M. J., Swindle T. D., Owen T., and Musselwhite D. S. 1994. Fractionated martian atmosphere in the nakhlites? *Meteoritics* 29:854–859.

Fanale F. P., Cannon W. A., and Owen T. 1978. Mars—Regolith adsorption and relative concentrations of atmospheric rare-gasses. *Geophysical Research Letters* 5:77–80.

Garrison D. H. and Bogard D. D. 2000. Cosmogenic and trapped noble gases in the Los Angeles martian meteorite (abstract). *Meteoritics & Planetary Science* 35:A58.

Gilmour J. D., Lyon I. C., Johnston W. A., and Turner G. 1994. RELAX—An ultrasensitive, resonance ionization mass spectrometer for xenon. *Review of Scientific Instruments* 65:617–625.

Gilmour J. D., Whitby J. A., and Turner G. 1998. Xenon isotopes in irradiated ALH 84001: Evidence for shock-induced trapping of ancient martian atmosphere. *Geochimica et Cosmochimica Acta* 62:2555–2571.

Gilmour J. D., Whitby J. A., and Turner G. 1999. Martian atmospheric xenon contents of Nakhla mineral separates: Implications for the origin of elemental mass fractionation. *Earth and Planetary Science Letters* 166:139–147.

Gilmour J. D., Whitby J. A., and Turner G. 2001. Disentangling xenon components in Nakhla: Martian atmosphere, spallation and martian interior. *Geochimica et Cosmochimica Acta* 65: 343–354.

Herd C. D. K. and Papike J. J. 2000. Oxygen fugacity of the martian basalts from analysis of iron-titanium oxides: Implications for mantle-crust interaction on Mars (abstract). *Meteoritics & Planetary Science* 35:A70.

Hohenberg C. M., Hudson B., M. K. B., and Podosek F. A. 1981. Xenon spallation systematics in the Angra dos Reis meteorite. *Geochimica et Cosmochimica Acta* 45:1909–1915.

Jagoutz E. 1991. Chronology of SNC meteorites. *Space Science Reviews* 56:13–22.

Jagoutz E., Sorowka A., Vogel J. D., and Wänke H. 1994. ALH 84001: Alien or progenitor of the SNC family. *Meteoritics* 29: 478–479.

Jones J. H. 1986. A discussion of isotopic systematics and mineral zoning in the shergottites: Evidence for a 180 Myr igneous crystallization age. *Geochimica et Cosmochimica Acta* 50:969–977.

Jones J. H. 1989. Isotopic relationships among the shergottites, the nakhlites and Chassigny. Proceedings, 19th Lunar and Planetary Science Conference. pp. 465–474.

Lodders K. 1998. A survey of shergottite, nakhlite, and Chassigny meteorites' whole-rock compositions. *Meteoritics & Planetary Science* 33:A183–A190.

Longhi J. 1991. Complex magmatic processes on Mars: Inferences from the SNC meteorites. Proceedings, 21st Lunar and Planetary Science Conference. pp. 695–709.

Marty B. and Marti K. 2002. Signatures of early differentiation of Mars. *Earth and Planetary Science Letters* 196:251–263.

Mathew K. J. and Marti K. 2001. Early evolution of martian volatiles: Nitrogen and noble gas components in ALH 84001 and Chassigny. *Journal of Geophysical Research* 106:1401–1422.

Mathew K. J. and Marti K. 2002. Martian atmospheric and interior volatiles in the meteorite Nakhla. *Earth and Planetary Science Letters* 199:7–20.

Mathew K. J., Marty B., Marti K., and Zimmermann L. 2003. Volatiles (nitrogen, noble gases) in recently discovered SNC meteorites, extinct radioactivities and evolution. *Earth and Planetary Science Letters* 214:27–42.

McSween H. Y. J. 1994. What we have learned about Mars from SNC meteorites. *Meteoritics* 29:757–779.

Miura Y. N., Nagao K., Sugiura N., Sagawa H., and Matsubara K. 1995. Orthopyroxenite ALH 84001 and shergottite ALH 77005—Additional evidence for a martian origin from noble gases. *Geochimica et Cosmochimica Acta* 59:2105–2113.

Mohapatra R. K. and Ott U. 2000. Trapped noble gases in Sayh al Uhaymir 005: A new martian meteorite from Oman (abstract). *Meteoritics & Planetary Science* 35:A113.

Murty S. V. S. and Mohapatra R. K. 1997. Nitrogen and heavy noble gases in ALH 84001: Signature of ancient martian atmosphere. *Geochimica et Cosmochimica Acta* 61:5417–5428.

Musselwhite D. S. and Swindle T. D. 2001. Is release of martian atmosphere from polar clathrate the cause of the nakhlite and ALH 84001 Ar/Kr/Xe ratios? *Icarus* 154:207–215.

Ott U. 1988. Noble gases in SNC meteorites: Shergotty, Nakhla, Chassigny. *Geochimica et Cosmochimica Acta* 52:1937–1948.

Ott U. and Lohr H. P. 1992. Noble gases in the new shergottite LEW 88516. *Meteoritics* 27:271.

Ott U., Lohr H. P., and Begemann F. 1988. New noble gas data for SNC meteorites: Zagami, Lafayette and etched Nakhla. *Meteoritics* 23:295–296.

Owen T., Biemann K., Rushneck D. R., Biller J. E., Howarth D. W., and Lafleur A. L. 1977. The composition of the atmosphere at the surface of Mars. *Journal of Geophysical Research* 82:4635–4639.

Ozima M. and Podosek F. A. 1983. *Noble gas geochemistry.* Cambridge: Cambridge University Press. 367 pp.

Podosek F. A. 1973. Thermal history of nakhlites by Ar-40-Ar-39 method. *Earth and Planetary Science Letters* 19:135–144.

Shih C. Y., Nyquist L. E., Bogard D. D., McKay G. A., Wooden J. L., Bansal B. M., and Wiesmann H. 1982. Chronology and petrogenesis of young achondrites, Shergotty, Zagami, and ALH A77005—Late magmatism on a geologically active planet. *Geochimica et Cosmochimica Acta* 46:2323–2344.

Shukolyukov A. and Begemann F. 1996. Pu-Xe dating of eucrites. *Geochimica et Cosmochimica Acta* 60:2453–2471.

Smith J. V. and Hervig R. L. 1979. Shergotty meteorite: Mineralogy, petrology and minor elements. *Meteoritics* 14:121–142.

Stöffler D., Ostertag R., Jammes C., Pfannschmidt G., Sen Gupta P. R., Simon S. B., Papike J. J., and Beauchamp R. H. 1986. Shock metamorphism and petrology of the Shergotty achondrite. *Geochimica et Cosmochimica Acta* 50:889–904.

Stolper E. M. and McSween H. Y. J. 1979. Petrology and origin of the shergottite meteorites. *Geochimica et Cosmochimica Acta* 43: 1475–1498.

Swindle T. D., Caffee M. W., and Hohenberg C. M. 1986. Xenon and other noble gases in shergottites. *Geochimica et Cosmochimica Acta* 50:1001–1015.

Swindle T. D., Grier J. A., and Burkland M. K. 1995. Noble gases in orthopyroxenite ALH 84001: A different kind of martian meteorite with an atmospheric signature. *Geochimica et Cosmochimica Acta* 59:793–801.

Swindle T. D., Hohenberg C. M., Nichols R. H., Olinger C. T., and Garrison D. H. 1989. Excess fission xenon in meteorites. *Meteoritics* 24:330–330.

Swindle T. D., Treiman A. H., Lindstrom D. J., Burkland M. K., Cohen B. A., Grier J. A., Li B., and Olson E. K. 2000. Noble gases in iddingsite from the Lafayette meteorite: Evidence for liquid water on Mars in the last few hundred million years. *Meteoritics & Planetary Science* 35:107–115.

Terribilini D. 2000. Edelgasisotopenanalysen und Bestrahlungsgeschichte von estraterrestrischen Gestein- und Metallproben. Ph.D. thesis, University of Bern, Switzerland.

Wiens R. C. 1988. Noble gases released by vacuum crushing of EET A79001 glass. *Earth and Planetary Science Letters* 91:55–65.

Wiens R. C. and Pepin R. O. 1986. Laboratory shock emplacement of low ambient pressure gases into basalt—Relation to EET A79001 trapped gas. *Meteoritics* 21:540–540.